Sensitivity Analysis of Magneto-Optic Imaging In Nondestructive Evaluation of Pipelines

Ibrahim Elshafiey* and Lalita Udpa**

*Electrical Eng. Dept., King Saud University, Riyadh, SA
**Electrical Eng. Dept, Michigan State University, Michigan, USA

ABSTRACT

Magneto-Optic Imaging (MOI) is a relatively new nondestructive evaluation modality that provides real time images of surface and subsurface features. In this technique, flux leakage maps associated with applied currents are recorded and monitored to locate material defects. Various factors affect the sensitivity of nondestructive evaluation using MOI including structure geometry, instrumentation parameters, and flaw characteristics. Computational modeling is presented in this research to characterize the sensitivity of MOI to material flaws. Three-dimensional finite element formulation is invoked to study the interaction of applied current and specimen under test. Results are shown of performance of MOI systems in detecting hidden flaws in pipeline configuration. Analysis considers a range of excitation source parameters and specimen defect characteristics. Accurate sensitivity analysis would help optimize MOI system design and promote its use in NDE applications in inspecting pipelines.

INTRODUCTION

Nondestructive evaluation (NDE) plays an essential role in assuring the integrity and safety of various engineering systems. Examples include nuclear power plants, aging aircraft, and oil industry. Various modalities have been adopted for NDE including radiography, eddy current, ultrasonics, magnetic methods and optical techniques. Every modality has its own advantages and disadvantages. Radiography techniques, for example, provide easy to interpret two dimensional scans. They require, however, precautions considering radiation hazards. Ultrasonic testing on the other hand depends on simple probes, providing single location measurements. Advanced systems are required to obtain two-dimensional ultrasonic scans and the scanning time is elongated.

Hybrid techniques can be invoked to optimize the performance of inspection system. An example is in magneto-optic imaging (MOI). The idea is to measure the interaction of magnetic field induced by applied current and optical light. The result is provided as two-dimensional images enhancing the interpretation of the testing and expediting the inspection process.

An important aid to NDE is the use of computer modeling techniques to predict relationships between defect size and the signal indicated by an appropriate detector. The techniques help design inspection instrumentation and choose optimum operating conditions [1].

In this paper, a case study is invoked of inspecting hidden flaws in pipelines. The configuration should be of interest to oil and natural gas industries. The structure implemented in the model assumes two pipes connected with a connector, whereas a crack is initiated in the inner surface of the pipes, as shown in Fig. 1.

Background on MOI principles as well as details of developed model and results are presented next.

MAGNETO-OPTIC EFFECT

Six magneto-optic effects are known [2], namely: Zeeman effect, inverse Zeeman effect, Voigt effect, Cotton-Mouton effect, Kerr magneto-optic effect and Faraday effect. Faraday effect discovered in 1845 is the one that is mostly used of these techniques. In his experiment, Faraday directed linearly polarized optical waves into glass block that is subject to large dc magnetic field. Polarization of light rotated as the beam propagated into glass.

Polarization rotation, commonly known as *Faraday rotation* is a direct consequence of the fact that refractive indices n_R and n_L for right-hand circularly polarized RHCP and left-hand circularly polarized LHCP light, respectively, are not equal in the presence of applied magnetic field. This can be explained by as a result of the disturbance that is caused in electron positions by external fields. In the absence of external fields, an electron is

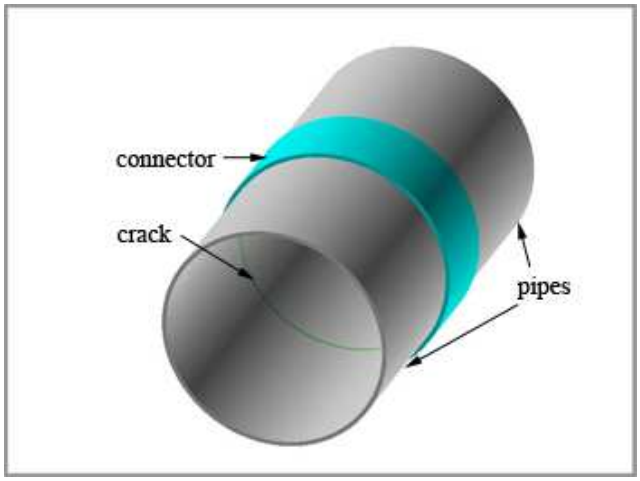

Fig. 1. Pipeline configuration with crack

bound to an equilibrium position due to forces caused by the nucleus as well as the lattice. In the presence of external magnetic field, however, a Lorentz force disturbs the electron position resulting in the fact that $n_R \neq n_L$.

Since a linearly polarized light can be considered as a summation of right and left circularly polarized components, the disturbance of corresponding refractive indices results in rotation of the polarization angle. For a wave that is linearly polarized in the x direction at z=0, and propagating in the z direction, the electric field vector is rotated by an angle $\varphi_F(z)$. For paramagnetic and diamagnetic materials, the angle of ration φ_F is linearly proportional to the component of the magnetic field intensity $\underline{H}$ in the direction of propagation $\underline{a}_K$,

$$\varphi_F(z) = V(\underline{H} \cdot \underline{a}_k)z \qquad (1)$$

where *V* is the Verdet constant.

In ferromagnetic materials, the rotation is expressed in terms of magnetization $\underline{M}$ [2], such that

$$\varphi_F(z) = K(\underline{M} \cdot \underline{a}_k)z \qquad (2)$$

and *K* is the Kundt constant.

MAGNETO-OPTIC IMAGING

MOI has been used to monitor defects in aircraft skin. Boeing and McDonnel Douglas have published procedures for use of MOI in 1992. Other companies such as Lockheed have also followed [3]. In aircraft inspection, time varying magnetic fields associated with the AC current passing through a planar induction foil induces a sheet of eddy current in the aircraft skin according to Faraday's law of electromagnetic induction. The operating frequency of MOI applications typically ranges from few hundred Hertz up to 100 kHz. The presence of rivets or defects diverts the eddy current from its uniform flow, and hence generates a normal magnetic field component, which can be measured using Faraday's magneto-optic effect. A magneto-optic sensor, placed parallel to the eddy current induction foil, is excited by a linearly polarized light. The plane of polarization undergoes rotation by an angle that depends on the local magnetic field intensity, and the specific Faraday rotation of sensor material. Perturbations in the magnetic field are monitored by analyzing rotation in light polarization.

Commercially available system [4] was first developed by Physical Research Inc. PRI, before purchasing the MOI technology, recently, by Quest Integrated, Inc [5]. The system included CCD video camera mounted on the imager, and the signal is directed to head-mounted display such that the inspector would monitor, on-line, defects inside the metal. Samples of MOI inspection images of a crack-free site, and a rivet with cracks in its site are shown in Fig. 2 [6].

(A) (B)

Figure 2. Samples MOI images. (a) defect free image, and (b) image of a rivet with cracks in its site. (after PRI)

Magneto-Optic Sensors

Exploration of materials for magneto-optical applications has primarily dealt with two different systems, the ferrimagnetic garnets and the amorphous rare earth-transition metal films. Careful studies of the effects of substituents (notably Bi and Pb) showed an increase in magneto-optic rotation while other substituents (such as Ca) were found to improve transparency [7]. Current sensors are made of a single crystal gadolinium gallium garnet (GGG) with an epitaxial thin film of bismuth-doped iron garnet. The substrate is typically 3-inch in diameter, and 0.02 inch-thick. Bismuth doped iron garnets give very large specific Faraday rotation.

COMPUTATIONL MODELING OF MOI

MOI depends on the values of induced magnetic field. Computational modeling can be used to test the feasibility of using MOI in detecting hidden flaws. In this paper, finite element modeling is used to simulate MOI inspection of hidden flaws in pipelines. Finite element depends on approximating the original continuous system by a system of discrete elements [8]. For harmonic finite element implementation, the source current and thus the field values vary sinusoidally with time. Electrical conductivity and magnetic permeability of materials in the solution region are single valued within each element. The formulation is written in terms of the magnetic vector potential $\underline{A}$, and electric scalar potential V. The magnetic flux density vector B and electric field intensity vector E are derived from $\underline{A}$ and V such that:

$$\underline{B} = \nabla x \underline{A} \tag{3}$$

$$\underline{E} = -\frac{\partial \underline{A}}{\partial t} - \nabla V \tag{4}$$

The domain space can be divided into two regions: Ω_1 for conducting materials of the pipes and connector and Ω_2 of the air region and crack region. The differential equations to be solved can be stated in terms of reluctivity ν, conductivity σ and source current density J_s as follows [9]

$$\nabla \times \nu \nabla \times \underline{A} + \sigma \frac{\partial \underline{A}}{\partial t} + \sigma \nabla V = 0 \quad \text{in } \Omega_1 \tag{5}$$

$$\nabla \times \nu \nabla \times \underline{A} = \underline{J}s \quad \text{in } \Omega_2 \tag{6}$$

The boundary conditions on surface Γ_{12} between $\Omega_1$and Ω_2 are stated as

$$n_1 \cdot \nabla \times \underline{A}_1 + n_2 \cdot \nabla \times \underline{A}_2 = 0 \tag{7}$$

$$\nu_1 \nabla \times \underline{A}_1 \times \underline{n}_2 + \nu_2 \nabla \times \underline{A}_2 \times \underline{n}_2 = 0 \tag{8}$$

where $\underline{n}_1$ and $\underline{n}_2$ are the outer normal to corresponding surface on regions Ω_1 and Ω_2.

The continuous variables $\underline{A}$, and V are approximated over a finite element. The general approximation is given as

$$\underline{A} = \sum_{i=1}^{M} N_i \underline{A}_i \qquad (9)$$

for the vector potential and

$$V = \sum_{i=1}^{M} N_i V_i \qquad (10)$$

where N_i stands for shape functions, and *M* is the number of nodes that define the element. Discretizing the problem the differential equations stated previously can be cast in the form of a linear system of equations.

MODELING RESULTS

A commercially available finite element package, ANSYS is used in the modeling. Fig. 2 presents two-dimensional mesh of a cross section of the configuration including the pipelines, the connector, the crack, in addition to the air inside and outside the pipe. The mesh has 1128 elements and 3487 nodes. The two dimensional mesh is then rotated to obtain three dimensional discretization. The resulting mesh consists of 22560 elements and 91445 nodes.

Two element types are considered. Elements corresponding to air and crack have nodal degree of freedom consisting of the three components of the magnetic vector potential A. Elements corresponding to the pipes and hte connector have scalar potential V degree of freedom, in addition to Ax, Ay and Az. Actual implementation assumes degree of freedom to be the time integration of *V*, rather than *V* itself. Source is applied as current injection on one side of the pipelines. The voltage degree of freedom is coupled on all nodes of the pipeline on the source injection side. Voltage degree of freedom is set to zero on the other side of the pipeline. As a boundary condition, the degrees of freedom of the outer nodes in air are set to zero. Resulting number of equations is 76799, and the

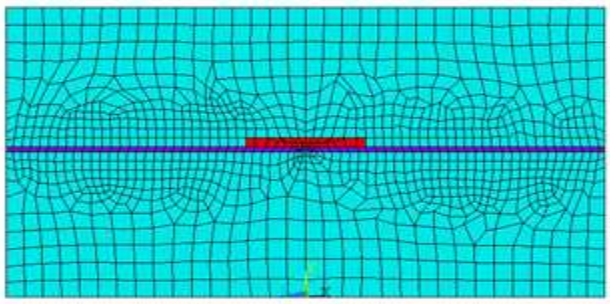

Fig. 3. Two-dimensional mesh.

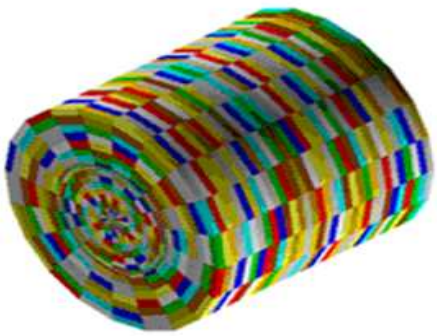

Fig. 4. Discretization of structure into 3D elements.

maximum wavefront of global matrix is 407.

The model is implemented for various excitation frequencies and different crack sizes. Time of one run of the model is around 10 minutes on a 3 GHz processor computer. Results are shown in Fig. 5 for three crack sizes. The width is fixed for all cracks to be 10 mm, and the depth is changed as 1 mm for the first crack, 2 mm for the second crack and 10 mm for the third crack. As for frequency variation, results are shown for 4 different frequencies: 100 Hz, 1 KHz, 10 kHz and 50 kHz respectively.

In Fig. 5, the horizontal axes correspond to distance from the epicenter of the crack. The vertical axes correspond to percentage variation of the normal component of $\underline{B}$ from baseline value calculated with no-crack condition. The $\underline{B}$ values are calculated 0.4 mm on top of the connector surface. As the figure shows, the main variation of the normal component of $\underline{B}$ occurs at the edges of the crack. At low source frequency there is a considerable change of $\underline{B}$ in the epicenter of the crack, which becomes less noticeable at larger frequencies.

DISCUSIONS AND CONCLUSIONS

Real time images of defects in pipelines can be monitored using magneto-optic imaging technology. The technique depends on exciting the specimen by a current and measuring the normal magnetic field component using Faraday magneto-optic effect. Sensitivity of the inspection to defect size and location can be obtained using finite

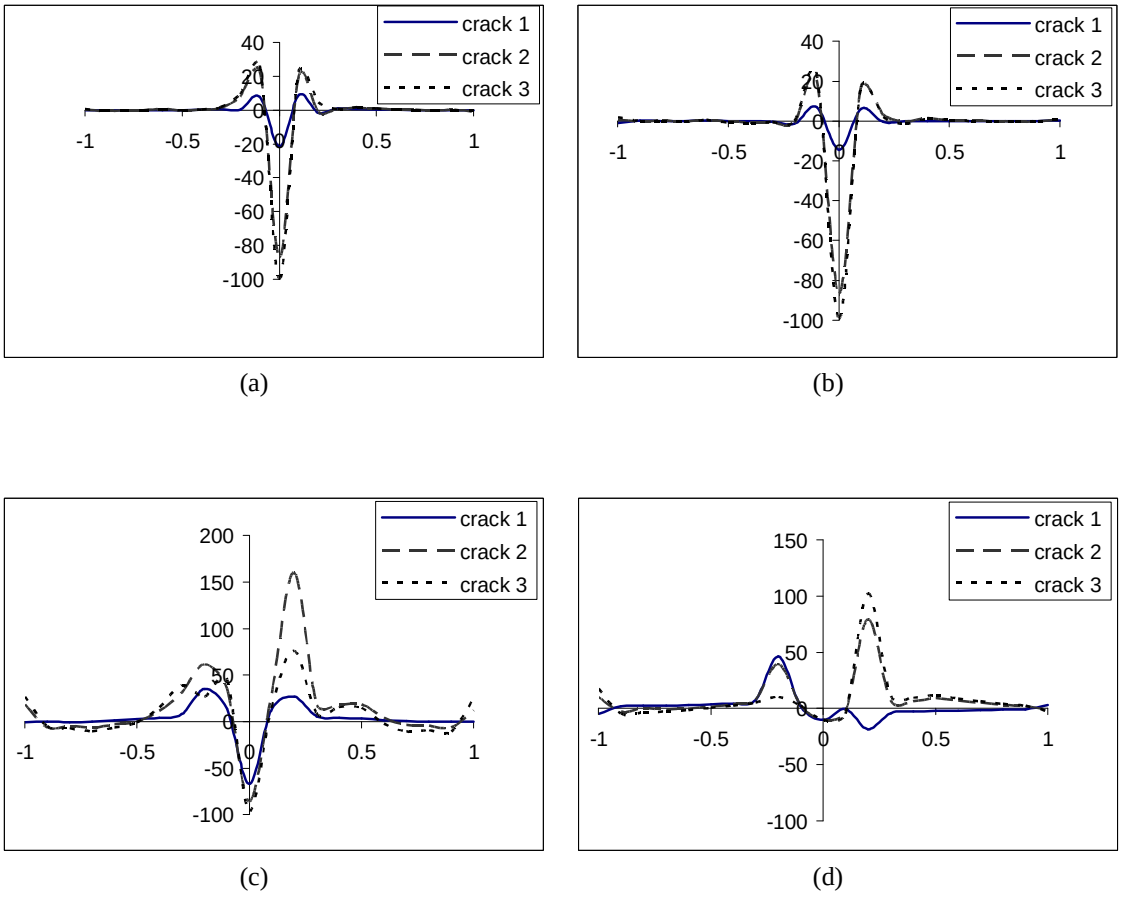

Fig. 5. Variation of normal component of $\underline{B}$ along a path 0.4 mm on top of the connector surface with three different subsurface cracks. The operating frequencies are 100 Hz (a), 1 kHz (b), 10 kHz (c) and 50 kHz (d).

element technique to model the interaction of the MOI source with the material.

Modeling results show that there is a considerable change in vertical component of the magnetic field, and that MOI is a powerful candidate for NDE of pipelines. Sensitivity of the inspection is found to be highly dependant on injected current frequency. MOI raw images can further be enhanced to increase inspection sensitivity by invoking digital image processing techniques. Special interest is currently directed in industry towards the automation of signal classification in nondestructive evaluation. Finite element modeling can help generate MOI simulated images needed for training the automatic signal classifiers.

REFERENCES

1. J. Blitz, *Electrical and Magnetic Methods of Nondestructive Testing*, Adam Higler, Bristol, 1991.
2. C. Chen, Elements of Optoelectronics & Fiber Optics, Irwin, Chicago, 1996.
3. Sandra Simms, “MOI: Magneto-Optic/Eddy Current Imaging”, Materials Evaluation, pp. 529-534, May, 1993.
4. D. Thome, Development of an Improved Magneto-Optic/Eddy-Current Imager, FAA report number DOT/FAA/AR-97/37, 1998.
5. Web site of Quest Integrated, Inc.: www.qi2.ocm.
6. Web site of Physical Research Inc: www.prind.com.
7. J.F. Dillon, Jr. "Magnetooptics and Its Uses," Journal of Mangnetism and Magnetic Materials, 31-34, pp. 1-9, 1983.
8. N. Ida, Numerical Modeling for Electromagnetic Non-Destructive Evaluation, Chapman & Hall, 1995.
9. O. Biro, and K. Preis, "On the Use the Magnetic Vector Potential in the Finite Element Analysis of Three-Dimensional Eddy Currents," IEEE Trans. on Magnetics, Vol. 25, pp. 3145-3159, 1989.